Journal of Membrane Science 599 (2020) 117682

Contents lists available at ScienceDirect

Journal of Membrane Science

journal homepage: http://www.elsevier.com/locate/memsci

Chemically reactive membrane crystallisation reactor for CO_2–NH_3 absorption and ammonium bicarbonate crystallisation: Kinetics of heterogeneous crystal growth

S. Bavarella [a], A. Brookes [b], A. Moore [c], P. Vale [d], G. Di Profio [e], E. Curcio [f], P. Hart [g], M. Pidou [a], E.J. McAdam [a,*]

[a] Cranfield Water Science Institute, Vincent Building, Cranfield University, Bedfordshire, MK43 0AL, UK
[b] Anglian Water, Thorpewood House, Peterborough, UK
[c] Northumbrian Water, Boldon House, Pity Me, Durham, UK
[d] Severn Trent Water, Coventry, UK
[e] Institute on Membrane Technology, National Research Council of Italy ITM-CNR, Rende, Italy
[f] Department of Environmental and Chemical Engineering, University of Calabria, Rende, Italy
[g] Centre for Energy and Power, Cranfield University, Bedfordshire, MK43 0AL, UK

ARTICLE INFO

Keywords:
Nucleation
Solid phase
Chemical absorption
Precipitation
Ammonia

ABSTRACT

The feasibility of gas-liquid hollow fibre membrane contactors for the chemical absorption of carbon dioxide (CO_2) into ammonia (NH_3), coupled with the crystallisation of ammonium bicarbonate has been demonstrated. In this study, the mechanism of chemically facilitated heterogeneous membrane crystallisation is described, and the solution chemistry required to initiate nucleation elucidated. Induction time for nucleation was dependent on the rate of CO_2 absorption, as this governed solution bicarbonate concentration. However, for low NH_3 solution concentrations, a reduction in pH was observed with progressive CO_2 absorption which shifted equilibria toward ammonium and carbonic acid, inhibiting both absorption and nucleation. An excess of free NH_3 buffered pH suitably to balance equilibria to the onset of supersaturation, which ensured sufficient bicarbonate availability to initiate nucleation. Following induction at a supersaturation level of 1.7 (3.3 M NH_3), an increase in crystal population density and crystal size was observed at progressive levels of supersaturation which contradicts the trend ordinarily observed for homogeneous nucleation in classical crystallisation technology, and demonstrates the role of the membrane as a physical substrate for heterogeneous nucleation during chemically reactive crystallisation. Both nucleation rate and crystal growth rate increased with increasing levels of supersaturation. This can be ascribed to the relatively low chemical driving force imposed by the shift in equilibrium toward ammonium which suppressed solution reactivity, together with the role of the membrane in promoting counter-current diffusion of CO_2 and NH_3 into the concentration boundary layer developed at the membrane wall, which permitted replenishment of reactants at the site of nucleation, and is a unique facet specific to this method of membrane facilitated crystallisation. Free ammonia concentration was shown to govern nucleation rate where a limiting NH_3 concentration was identified above which crystallisation induced membrane scaling was observed. Provided the chemically reactive membrane crystallisation reactor was operated below this threshold, a consistent (size and number) and reproducible crystallised reaction product was collected downstream of the membrane, which evidenced that sustained membrane operation should be achievable with minimum reactive maintenance intervention.

1. Introduction

The use of packed columns for the absorption of carbon dioxide (CO_2) has received significant attention over the past decade, for their potential to facilitate carbon capture and storage (CCS) as well as enabling CO_2 separation from biogas for the production of biomethane;

* Corresponding author.
E-mail address: e.mcadam@cranfield.ac.uk (E.J. McAdam).

https://doi.org/10.1016/j.memsci.2019.117682
Received 4 July 2019; Received in revised form 7 November 2019; Accepted 20 November 2019
Available online 22 November 2019

this latter application representing one of the fastest growing areas for gas-liquid separation technology [1]. In both applications, chemically reactive solvents have been employed as a method of process intensification [2,3].

Aqueous ammonia has been shown to achieve higher CO_2 loadings than sterically free primary alkanolamines such as monoethanolamine [4]. However, the absorption and reaction kinetics between CO_2 and aqueous ammonia are complex [5], and the resultant species formed in a CO_2–NH_3–H_2O system are difficult to predict, despite the commercial significance of the overall reaction in the industrial production of crystalline ammonium bicarbonate (NH_4HCO_3), for the food, fertilizer, pharmaceutical and manufacturing sectors, due to differences in solution chemistry, reactor configuration and driving force imposed to initiate a phase change [6,7]. Veiga et al. [6] were amongst the first to report on a three phase (gas-liquid-solid) system for the controlled production of crystalline NH_4HCO_3 in which governance over crystal size and morphology was evaluated. The overall chemical reaction can be described as:

$$NH_4^+(aq) + HCO_3^-(aq) \leftrightarrow NH_4HCO_3(s) \quad (1)$$

In packed column studies for NH_3–CO_2 absorption, the formation of an NH_4HCO_3 solid was also considered as this has the potential to improve CO_2 solvent capacity, thereby reducing the mass flow of stripper solution and lowering the specific energy demand for CCS [8]. However, managing formation and recovery of the crystalline solid within packed columns was found to be difficult [9], and demands explicit investigation of the underpinning science to define the kinetics of solids formation in CO_2–NH_3–H_2O systems for CO_2 absorption [10,11]. Subsequent investigations of NH_3–CO_2 absorption for CCS have therefore sought to implement strategies that eliminate solid phase formation to obviate clogging of the packed media bed [8,12].

Several authors have now investigated microporous hollow-fibre membrane contactors (HFMC) for the absorption of CO_2 into ammonia [13–15]. In membrane contactors, the hydrophobic membrane permits non-dispersive contact between the gas phase (CO_2) and NH_3 rich solvent, with the gas filled pores of the microporous membrane mediating CO_2 transport from gas to liquid phase. Whilst inclusion of the membrane increases the overall resistance to mass transfer, the increase in specific surface area afforded by membrane contactors, provides a process intensification of over an order of magnitude compared with packed columns [16]. McLeod et al. [3] successfully evidenced that the nucleation and growth of crystalline ammonium bicarbonate on the solvent-side (shell-side) of a microporous HFMC was feasible in a CO_2–NH_3–H_2O system. In this proposed application for biogas upgrading, the reaction enabled separation of ammonia from wastewater and the formation of a new by-product to provide new value for the water industry [15]. Unlike in packed columns, the driving force for crystallisation is facilitated by counter-current diffusion of CO_2 and NH_3 into a chemically reactive concentration boundary layer developing at the solvent-membrane interface. The authors proposed that the membrane behaved as a physical substrate to lower the free energy barrier sufficient to initiate nucleation at the entrance of the pores where gas, liquid and solid (the membrane) interact such that heterogeneous nucleation was initiated in a controlled pathway [3,17,18]. The applied drag force employed within the laminar conditions used within membrane crystallisation has often been shown to be sufficient to harvest crystals and avoid long term crystal deposition at the membrane surface, which has been accounted for by the nonspecific and reversible chemical interaction between the membrane and solute [17].

The improved governance over nucleation provided by the membrane, coupled with the advantage of partitioning of the crystalline NH_4HCO_3 into the liquid phase, rather than a two-phase fluid as with packed columns, presents a simpler and more controlled method for reaction product recovery. However, whilst the thermodynamic behaviour of the CO_2–NH_3–H_2O system has been generally described, neither the solution chemistry required to initiate heterogeneous nucleation, or the crystallisation kinetics of a chemically reactive membrane crystalliser have been determined, which help to identify suitable boundary conditions for exploitation in CO_2 separations, as well as to indicate downstream processing requirements for product recovery. Supersaturation is the driving force for both nucleation and growth and the rate at which an excess of solute is achieved, is dependent upon the flux [17]. In this configuration, chemical reactivity will define flux, thus the free ammonia concentration will influence the kinetic trajectory of the final crystalline product. Whilst membrane assisted crystallisers have been developed using osmotic or vapour pressure gradient as the driving force, the only chemically reactive membrane crystallisation reactor reported to date used the membrane to facilitate mixing of two solutions [19]. The proposed configuration therefore represents a new chemically reactive membrane crystallisation reactor (CR-MCR) configuration. In this study we aim to characterise the chemistry and crystallisation kinetics underpinning crystal nucleation and growth in a membrane contactor for CO_2 absorption using NH_3, to enable consistent and reproducible recovery of the final crystalline solid reaction product. Specific objectives are to: (i) characterise the kinetics of crystal nucleation and growth in a chemically reactive membrane crystallisation reactor, driven by gas phase reaction; (ii) establish the significance of driving force on membrane crystallisation through variation in ammonia concentration; (iii) identify the chemistry needed to initiate nucleation in CR-MCR for ammonia mediated CO_2 separation; and (iv) provide confirmation of the reaction product identity and populate a mass balance to validate the successful separation of the crystalline reaction product from the membrane.

2. Materials and methods

2.1. Fabrication, equipment setup and operation

The module comprised of a single 165 mm long polypropylene (PP) micro-porous hollow-fibre membrane (Membrana GmbH, Wuppertal, Germany) with a nominal pore size of 0.2 μm and membrane area of 9.33×10^{-4} m^2 (based on the outer diameter) (Table 1).

The hollow-fibre membrane was potted in epoxy resin (Bostick Ltd., Stafford, UK) and sited within a 12 mm diameter channel within the Perspex cell (Fig. 1). To allow direct observation of shell-side

Table 1
Dimensions and characteristics of the hollow-fibre membrane.

Fibre characteristics		
Membrane material	–	polypropylene
Inner diameter	mm	1.2
Outer diameter	mm	1.8
Wall thickness	μm	300
Active length	mm	165
Surface area[b]	m^2	9.33×10^{-4}
Nominal pore size[a]	μm	0.2
Lumen cross sectional area	m^2	1.13×10^{-6}
Shell side characteristics		
Height	mm	5
Width	mm	12
Shell cross sectional area	m^2	6.0×10^{-5}
Priming volume	ml	11.0
Operational characteristics		
Flow regime		Counter-current
Shell-side		1, 1.9, 3.3, 4.6 M NH_3 (aq)
Lumen-side		99.8% CO_2
Liquid temperature	°C	5–7
Gas temperature	°C	18–20
Liquid velocity	m s^{-1}	0.06
Gas velocity	m s^{-1}	14.7
Gas humidity	%	38

[a] Data provided by manufacturer.
[b] Based on fibre outer diameter.

crystallisation, a viewing window was engineered into a recess within the upper section of the cell [20]. A Nikon SMZ-2T stereomicroscope with a 0.5x objective lens (Nikon UK Ltd., Surrey, UK) was fixed above the viewing window and images captured with a high-resolution camera (Leica EC3 Microsystems, Milton Keynes, UK). The limit of detection for direct observation is around 3 μm [45]. The technique therefore permits resolution of crystal growth above this size, and not of the determination of nucleation. Membrane experiments were conducted sacrificially for each supersaturation level reached (C/C*). The supersaturation level (C/C*) is defined as the ratio between the CO_2 absorbed into solution and the CO_2 required to form ammonium bicarbonate at the solubility limit. Due to the Gibbs free energy demanded to undergo a phase change, in addition to the dependency on the carbonate system equilibria, an induction time can be expected such that ammonium bicarbonate crystallisation will proceed at a C/C* greater than one. For each supersaturation level, a new single hollow-fibre was mounted into the Perspex cell. Sacrificial experiments were conducted in triplicate for each supersaturation level, and the mean and standard deviation reported.

Carbon dioxide (99.8%, BOC gases, Ipswich, UK) was introduced into the lumen of the hollow-fibre at a flow rate of 1000 ml min^{-1} using a laminar mass flow controller (0.01–1 L min^{-1}, Roxspur Measurement and Control Ltd., Sheffield, UK). Absorbent was pumped counter-current on the shell-side of the membrane at 200 ml min^{-1} with a peristaltic pump (520Du, Watson-Marlow Ltd., Falmouth, UK). The absorbent temperature was fixed at 5 °C with a refrigerated bath and circulator (R1 series, Grant Instruments Ltd., Cambridge, UK). Gas and liquid phase temperatures were measured across the membrane system (K-type thermocouples, Thermosense Ltd., Bucks, UK). Inlet temperatures for the gas and liquid phase were 20 °C and 5 °C respectively. The liquid temperature was selected as this reduces the solubility limit for ammonium bicarbonate, to induce crystallisation earlier, and also reduced the saturation vapour pressure for ammonia. Temperature losses across the membrane were noted to be around 0.4 ± 0.2 °C for both liquid and gas.

2.2. Chemical preparation, sampling and analysis

Absorbent ammonia concentrations ranging between 1.0 and 4.6 molNH_3 L^{-1} (M NH_3), were prepared through addition of aqueous NH_3 concentrate (35% Fisher Chemicals, Loughborough, UK) to de-ionised water (15.0 MΩ cm^{-1}). The absorbent pH was fixed at pH 10 with addition of hydrochloric acid (HCl, 37%, Fisher Scientific, Loughborough, UK) as this is typical of the pH employed in aqueous ammonia packed column processes [21]. Ammonia concentration was confirmed using an ammonium cell test which pre-acidifies the sample (VWR International Ltd., Poole, UK) before determination by spectrophotometry (Spectroquant Nova 60, Merck-Millipore, Darnstadt, Germany). A 1000 ml bubble flow meter (SKC, Blandford Forum, UK) was used to measure gas flow rate in order to calculate CO_2 flux (J_{CO2}, mol m^{-2} s^{-1})Eqn 2:

$$J_{CO_2} = \frac{\left(Q_{G,\ in} - Q_{G,\ out}\right) \times 273.15 \times 1000}{22.4 \times A_m T_G} \quad (2)$$

where $Q_{G,\ in}$ and $Q_{G,\ out}$ are the inlet and outlet gas flow rates (m^3 s^{-1}) respectively, A_m is the membrane surface area (m^2) and T_G is the gas temperature (K) [22]. The error for gas flow measurement was less than 2% of the reported value. Absorption solvent pH was monitored using a Jenway epoxy bodied pH electrode (Jenway 4330, Cole-Parmer, Stone, UK). The development of bicarbonate in solution was determined by UV absorbance at 215 nm (Jenway 6715, Cole-Parmer, Stone, UK) which corresponds to the absorption region for bicarbonate [23,46,47]. A crystal size distribution was developed for each sacrificial experiment which corresponded to a specific level of supersaturation (C/C*). Crystallisation data produced at each supersaturation level is representative of three individual experiments, in which three crystal size distributions were derived for each individual experiment. Prior to counting, the absorbent was filtered through a 0.45 μm filter (Whatman, Camlab Ltd., Cambridge, UK) and then immersed in anhydrous alcohol to minimise agglomeration [6]. The crystals were transferred onto a microscope slide consisting of a 1 mm counting grid, and placed under an optical microscope (Optech Microscope Services Ltd., Thame, UK) equipped with PL 5/0.12 lens and digital camera (Infinity 3, Lumenera, Ottawa, Canada). Images were analysed with image processing software (Image Pro Plus, Media Cybernetics, Cambridge, UK) to determine crystal number and size. Around 50 crystals were quantified with each image and a minimum of 600 crystals counted to develop one size distribution to minimise standard error [24]. A Siemens D5005 X-ray diffractometer

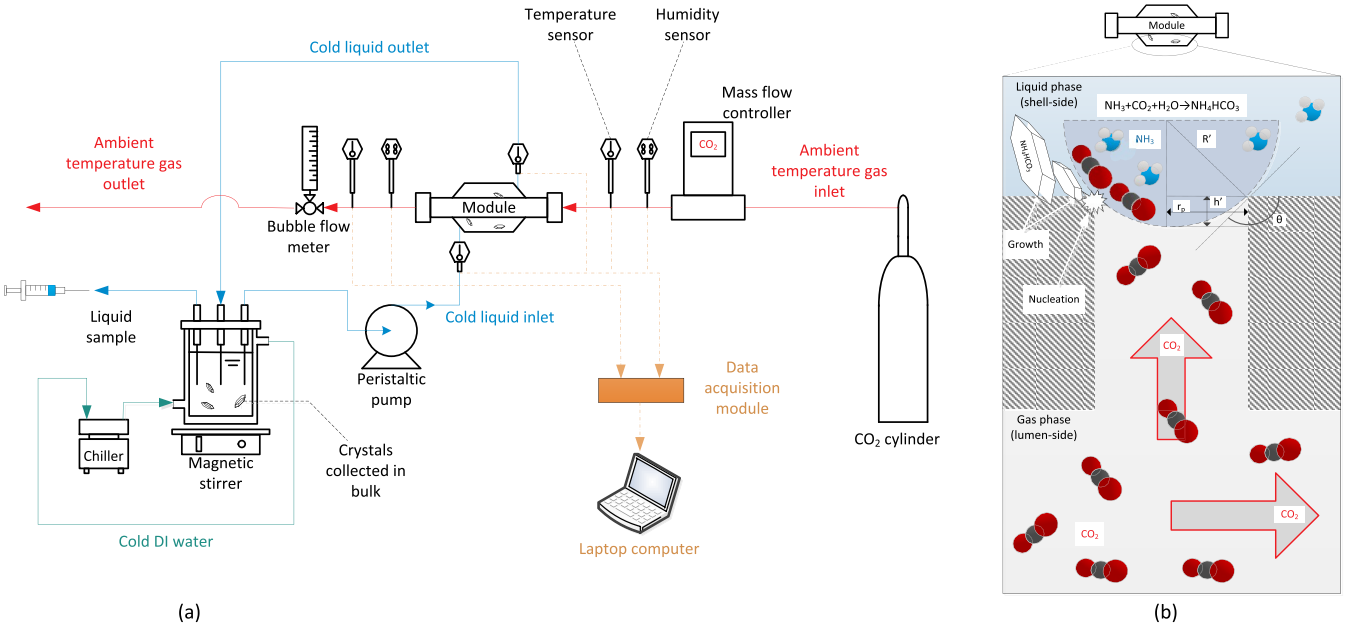

Fig. 1. (a) Experimental setup for the chemically reactive membrane crystallisation reactor; and (b) gas–liquid membrane crystallisation where CO_2 absorbed within NH_3 rich solution induces shell side supersaturation leading to nucleation and growth of NH_4HCO_3 product. (Both NH_3(g) and H_2O(v) could be transported from the shell side to the lumen side).

with Cu Ka1 radiation (Bruker UK Ltd., Coventry, UK) was used for crystal analysis, using a step size of 0.04° with diffraction patterns recorded in the 2θ range 15–40° [25].

2.3. Chemistry of the NH_3–CO_2–H_2O system

The absorption of carbon dioxide into aqueous ammonia solutions is thermodynamically controlled by the following equilibria [26,27]:

$$CO_2(g) \leftrightarrow CO_2(aq) \quad (3)$$

$$NH_3 \leftrightarrow NH_3(g) \quad (4)$$

$$H_2O \leftrightarrow H_2O(v) \quad (5)$$

Upon absorption of CO_2 into solution, the interactions between CO_2 and water can be described by:

$$CO_2(aq) + H_2O \leftrightarrow H_2CO_3 \quad (6)$$

$$CO_3^{2-} + H^+ \leftrightarrow HCO_3^- \quad (7)$$

$$HCO_3^- + H^+ \leftrightarrow H_2CO_3 \quad (8)$$

$$OH^- + H^+ \leftrightarrow H_2O \quad (9)$$

The relative proportion of dissolved CO_2 available as carbonate (CO_3^{2-}), bicarbonate (HCO_3) or carbonic acid (H_2CO_3) is dependent upon solution pH, assuming a fixed liquid temperature of 5 °C (Fig. 2).

The equilibrium between unprotonated ammonia (NH_3) and protonated ammonium (NH_4^+) is similarly dependent on solution pH (Fig. 2):

$$NH_3 + H^+ \leftrightarrow NH_4^+ \quad (10)$$

Wang et al. [28] investigated NH_3–CO_2 reaction kinetics in the liquid phase, comprising the reversible reactions of ammonium carbamate and carbamic acid formation:

$$CO_2(aq) + NH_3 \leftrightarrow NH_2COOH \quad (11)$$

$$NH_2CO_2^- + H^+ \leftrightarrow NH_2COOH \quad (12)$$

Five solid reaction products may form within the NH_3–CO_2–H_2O system [9], ammonium bicarbonate ($NH_4HCO_{3(s)}$, C* 200 kg m^{-3}), ammonium carbonate ($(NH_4)_2CO_{3(s)}$, C* 300 kg m^{-3}), ammonium sesquicarbonate ($(NH_4)_2CO_3{\cdot}2NH_4HCO_{3(s)}$, highly soluble), ammonium carbamate ($NH_2COONH_{4(s)}$, C* 600 kg m^{-3}) and ice. Ammonium bicarbonate is thermodynamically favoured at lower ammonia concentrations due to the lower solubility of the salt (Equation (1) [5]).

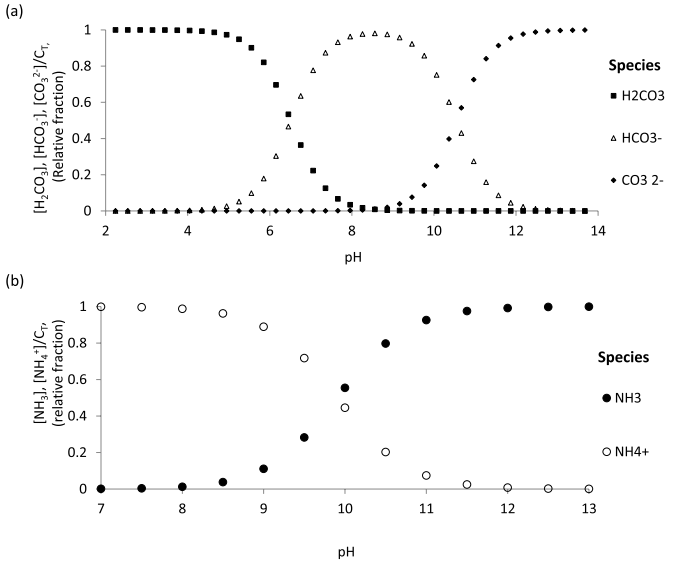

Fig. 2. Dependency of: (a) carbonate equilibria; and (b) ammonium-ammonia equilibrium on pH, for a fixed solution temperature of 5 °C in a closed system. Additional information available in appendix.

2.4. Crystallisation kinetics

In a supersaturated solution, the nucleation rate (B) and crystal growth rate (G) can be determined by Ref. [29]:

$$B = K_B G^b \quad (13)$$

$$G = K_G\left(c_{fm} - c^*\right)^g \quad (14)$$

where K_B (No m^{-3-b} s^{-1+b}; No = crystal number) and K_G (kg^{-g} m^{3g+1} s^{-1}) are the rate constants for nucleation and growth respectively, while c_{fm} and c* (kg m^{-3}) are the CO_2(aq) concentrations adjacent to the membrane surface and the equilibrium-saturated concentration at the membrane wall. Exponents *g and b* can be obtained from experimental data regression. Through determining the change in crystal number (ΔN) over a prescribed time period (Δt), the average nucleation rate becomes:

$$B(L,t) = \Delta N / \Delta t \quad (15)$$

Applying the experimentally derived values for B, into the logarithmic transformation of Equation (13), then permits determination of the kinetic nucleation constant K_B and exponent b from the intercept and slope respectively:

$$\log B = \log K_B + b \log G \quad (16)$$

Similarly, crystal growth rate can be defined as the change in size (m) over a prescribed time period (Δt), thus the average growth rate becomes:

$$G(L,t) = \Delta L / \Delta t \quad (17)$$

Following the determination of G from the linear slope [30], the crystal growth rate constant K_G and the exponent *g* can then be respectively derived from the intercept and slope of Equation (14), following logarithmic transformation:

$$\log G = \log K_G + g \log\left(c_{fm} - c^*\right) \quad (18)$$

3. Results

3.1. Impact of ammonia concentration on shell-side ammonium bicarbonate crystallisation

Carbon dioxide absorption was determined at four liquid phase ammonia concentrations ranging 1.0 to 4.6 molNH_3 L^{-1} with the NH_3 solution in recirculation (Fig. 3a). For each NH_3 concentration, CO_2 flux followed a similar two-stage profile, characterised by a rapid initial decline in CO_2 flux followed by a slow progressive decline in CO_2 flux. Whilst the initial CO_2 flux was lower for the 1 M NH_3 solution, the flux profile was similar for NH_3 solutions ranging 1.9–4.6 M. A spike in CO_2 flux was observed for the 4.6 M NH_3 solution, corresponding to a supersaturation level of 1.2 (Fig. 3b) and was coincident with the onset of substantive shell-side crystallisation which covered the membrane surface (Fig. 4). Within the 3.3 M NH_3 solution, shell-side crystallisation was observed at C/C* 1.7, with no observable impact on CO_2 flux. Shell-side crystallisation did not occur in NH_3 solutions ranging 1–1.9 M.

3.2. Chemistry governs induction of NH_4HCO_3 in CO_2–NH_3–H_2O system

As CO_2 absorption progressed, the solution pH declined (Fig. 5a). The reduction in pH was more evident for the lower ammonia

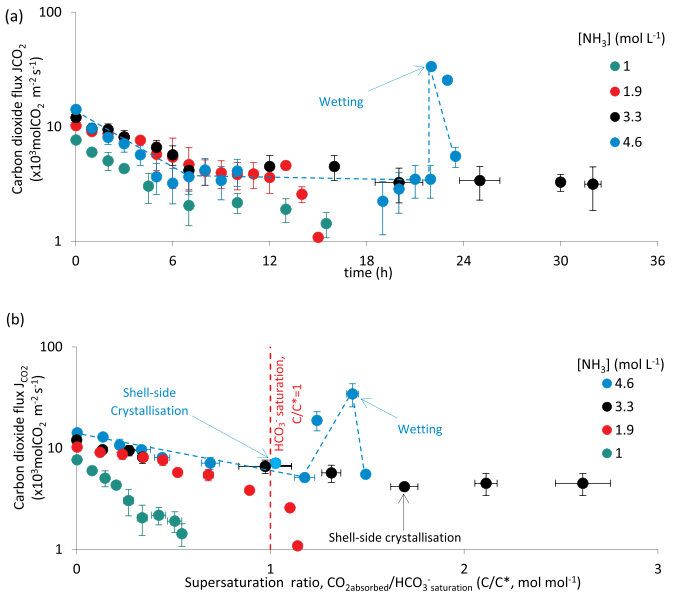

Fig. 3. Carbon dioxide (CO_2) flux determined for the polypropylene membrane with four concentrations of NH_3 absorbent (1–4.6 M NH_3) whilst operating absorbent in recirculation. Flux data plotted versus: (a) time; and (b) the supersaturation level (C/C*), which assumes complete conversion of CO_2 to HCO_3^-. Error bars represent standard deviation of sacrificial experiments undertaken in triplicate at each supersaturation level. Conditions: G/L 5; V_G 14.7 m s^{-1}; V_L 0.06 m s^{-1}; Liquid temperature 5 °C; Gas temperature 20 °C.

concentrations (1 and 1.9 M) despite the absorption of an equivalent amount of CO_2. To illustrate, a minimum pH value of 7.4 was reached at C/C* 0.55 with 1 M NH_3 absorbent, whilst that pH was reached at C/C* 2.60 for the 4.6 M NH_3 solution. However, normalisation of the cumulative CO_2 absorption data to the initial free ammonia concentration of solution (CO_2 solution loading, mol mol^{-1}) evidenced that the reduction in pH exhibits an analogous trend independent of initial NH_3 solution concentration (Fig. 5b). Shell-side crystallisation occurred at CO_2 loadings of 0.77 and 0.44 for 3.3 and 4.6 molNH_3 L^{-1} respectively.

The arising pH data was developed to estimate ammonia and bicarbonate equilibria during CO_2 absorption (Fig. 6).

The ammonia-ammonium equilibrium had shifted primarily toward NH_4^+ for each absorbent at supersaturation (C/C*, 1), independent of initial NH_3 concentration (Fig. 6). During the initial CO_2 absorption phase, the carbonate equilibrium shifts toward bicarbonate, due to the decrease in solution pH. However, as solution pH continued to decline with further CO_2 absorption, the water-CO_2 equilibrium shifts away from bicarbonate toward carbonic acid. For the lower NH_3 solution concentrations, this results in a peak in HCO_3^- concentration in advance of supersaturation (C/C*, 1). This was corroborated by UV_{215nm} in which the bicarbonate concentration was noted to peak for both the 1.0 and 1.9 M NH_3 solutions prior to supersaturation, and was evidently a contribution of the initial ammonia concentration (Fig. 6b and c). The UV_{215nm} absorbance provided a surrogate for HCO_3^- concentration and demonstrated the 4.6 M NH_3 solution to comprise the highest concentration at the point of supersaturation.

3.3. Kinetics of nucleation and growth for chemically assisted membrane crystallisation

For the 3.3 M NH_3 solution, an increase in crystal number and crystal size was observed with an increase in supersaturation level and was coincident with a decrease in UV_{215nm} (Fig. 7). The average crystal growth rate (G) was determined at each supersaturation level, which enabled derivation of the crystal growth rate constant K_G 1.7 × 10^{-14} kg^{-g} m^{3g+1} s^{-1} and exponent g, 2.6 (Fig. 8). The nucleation rate (B) was also

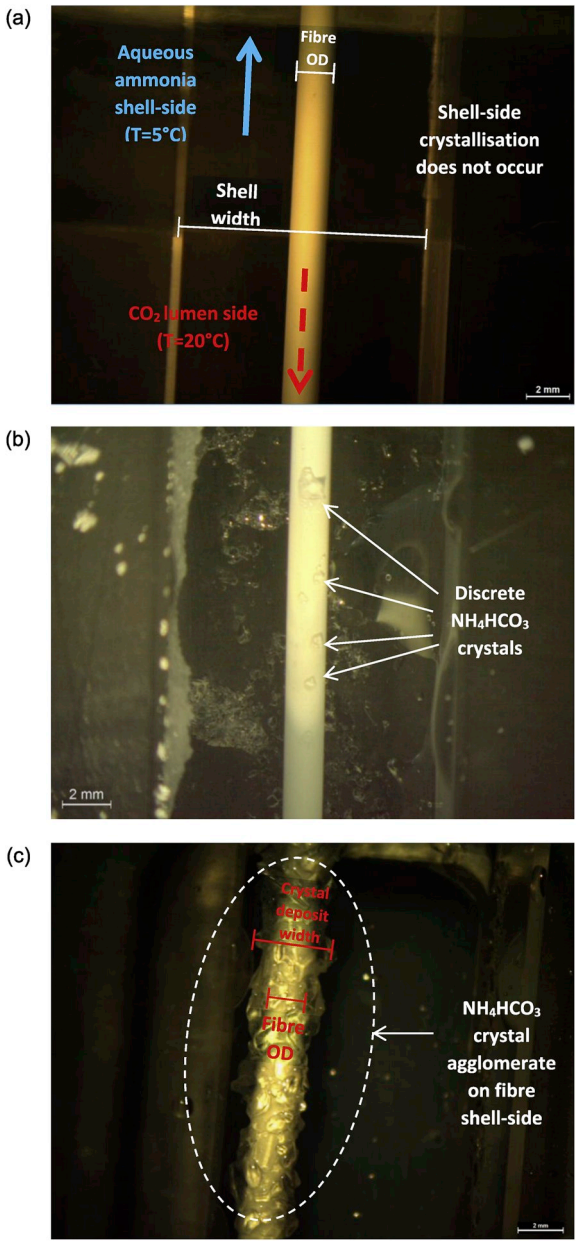

Fig. 4. Direct observation of membrane surface crystallisation in real time once supersaturation (C/C*) exceeded 1. Aqueous ammonia concentrations of: (a) 1.9 M; (b) 3.3 M; (c) 4.6 M. Conditions: G/L 5; V_G 14.7 m s^{-1}; V_L 0.06 m s^{-1}.

determined at each supersaturation level, to provide the nucleation rate constant K_B 7.1 × 10^8 No m^{-3-b} s^{-1+b} and exponent b 0.4. A nitrogen mass balance was undertaken according to:

$$\text{Nitrogen balance} = \frac{C_{b,f} + C_{cry}}{C_{b,i}} \quad (19)$$

where $C_{b,i}$ and $C_{b,f}$ are the initial and final ammoniacal nitrogen concentrations, and C_{cry} is the nitrogen concentration contained within the crystal. The nitrogen mass balance indicated that >99% of the nitrogen reduction in the absorbent was contained within the recovered crystalline product. X-ray diffraction was used to compare pure ammonium bicarbonate to crystals produced following CO_2 absorption into 3.3 M NH_3 solution, which evidenced crystals obtained through the CR-MCr to be ammonium bicarbonate (Fig. 9).

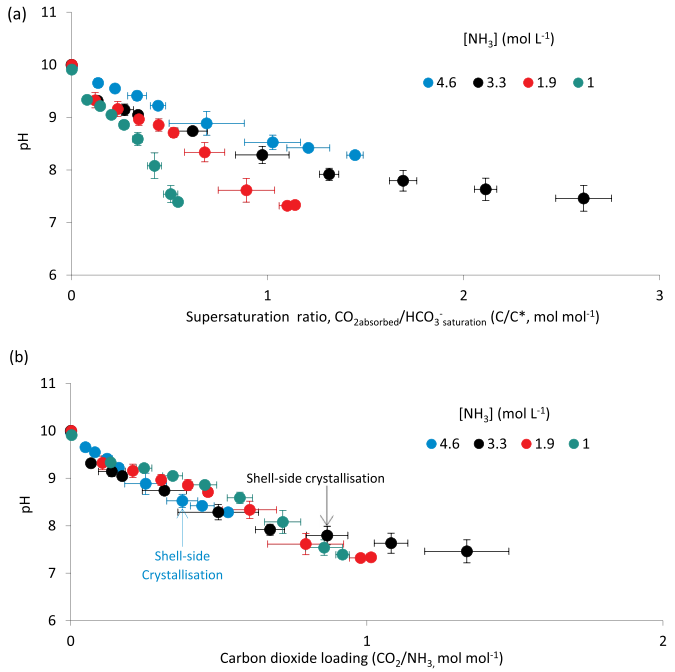

Fig. 5. Reduction in pH observed following progressive CO_2 absorption, analysed by: (a) supersaturation level; and (b) carbon dioxide loading normalised for initial ammonia concentration. Error bars indicate standard deviation from sacrificial experiments undertaken in triplicate at each supersaturation level. Liquid temperature 5 °C; Gas temperature 20 °C.

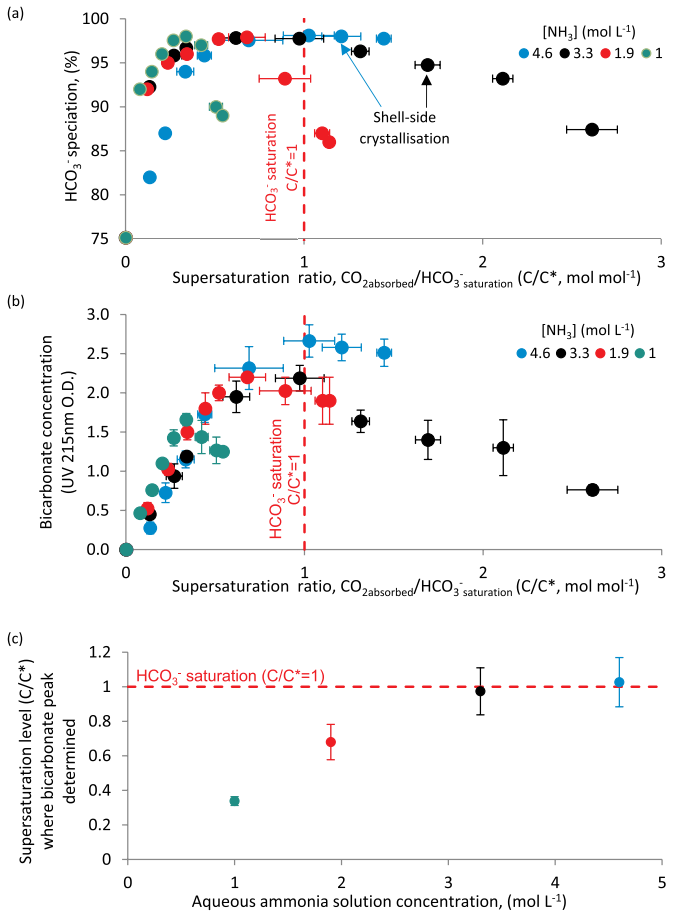

Fig. 6. Ongoing CO_2 absorption lowers pH which shifts carbonate equilibria generating a dynamic bicarbonate concentration: (a) bicarbonate speciation determined from literature equilibria data; (b) bicarbonate concentration determined at UV215nm, which confirms shift in HCO_3^- speciation and indicates relative concentration; and (c) the supersaturation level at which the peak in bicarbonate concentration is achieved. Error bars indicate standard deviation obtained from sacrificial experiments carried out in triplicate for each ammonia concentration. Liquid temperature 5 °C; Gas temperature 20 °C.

4. Discussion

In this study, the underpinning chemistry required to simultaneously absorb CO_2 and initiate nucleation of crystalline ammonium bicarbonate in a hollow-fibre membrane contactor has been ascertained, and the kinetics of heterogeneous nucleation and crystal growth determined, which evidence the mechanism for chemically reactive membrane crystallisation. Both crystal population density and crystal size increased with increasing levels of supersaturation (Fig. 8). This is in contrast to Veiga et al. [6] who crystallised ammonium bicarbonate in batch and observed a decline in crystal population density with particle size which is characteristic of conventional crystalliser configurations where homogeneous primary and secondary nucleation is favoured, due to the initial insufficiency of an immediate substrate [31,32]. The increase in population density observed in the present study (Fig. 8), in parallel with crystal growth, is indicative of sustained primary heterogeneous nucleation, promoted by the membrane substrate through a reduction in the free energy barrier. Di Profio et al. [33] also identified an increase in population density following supersaturation when operating membrane crystallisation for lysozyme recovery through an osmotic gradient. However, as their process was operated in batch, nucleation rate declined due to solute consumption at increasing levels of supersaturation for all but the lowest driving force. Whilst nucleation rates cannot be directly compared due to geometric differences amongst other considerations, the nucleation rate constant in this study was 7.1×10^8 No m^{-3-b} s^{-1+b} which is ten orders of magnitude below that reported by Curcio et al. [32] for a conventional crystalliser (Fig. 8). It is therefore asserted that the increasing nucleation rate and growth rate observed at increasing levels of supersaturation is due to: (i) the low driving force of the chemical reaction, which limited consumption of NH_3 in the initial phase of crystallisation; and (ii) the counter-current diffusion of CO_2 and NH_3 into the concentration boundary layer, which provided consistent replenishment of reactant to the site of preferential nucleation. This latter contribution is a unique facet of this chemically reactive membrane crystallisation reactor configuration. For the 4.6 M NH_3 solution, encrustation (or scaling) of the fibre occurred too quickly for the nucleation rate to be determined (Fig. 4). Chen et al. [29] asserted that crystallisation induced scaling arose from Ostwald ripening in which an agglomeration of fine particles occurred immediately after nuclei breeding, followed by the supported growth of coarser crystals through supply of small crystal particles that become more stable on the membrane surface. As the CO_2 flux profiles for both 3.3 and 4.6 M NH_3 solutions (Fig. 3) were similar, it is the free ammonia concentration and not CO_2 transport which determines the nucleation rate. It is suggested for this study, that the higher NH_3 concentration increased nucleation rate which induced an analogous effect to Ostwald ripening. The resultant effect was a change in surface contact angle which subsequently induced wetting and a breakthrough of solution NH_3 into the gas phase which temporarily increased flux (Fig. 3 [34]). In contrast, whilst several discrete crystals were observed to have formed on the membrane fibre at 3.3 M (Fig. 4b), most crystals were collected downstream of the membrane, which was confirmed by nitrogen mass balance. When coupled with the consistent flux profiles sustained over the duration of experiments, this would suggest that provided nucleation rate can be specific below a critical threshold, sustained membrane operation should be achievable with minimum reactive maintenance intervention.

The highest CO_2 flux recorded was similar to that of McLeod et al. [3] who used a wider pore size PTFE membrane for CO_2–NH_3 absorption. For initial NH_3 concentrations equal to or above 1.9 M, CO_2 flux was

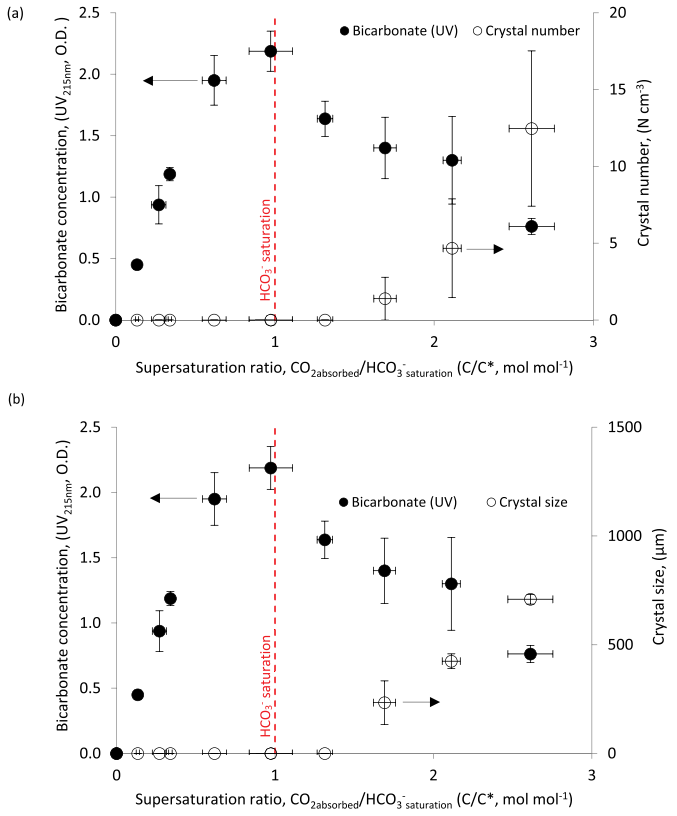

Fig. 7. Transition in (a) crystal number; and (b) crystal size, determined at progressive levels of supersaturation (saturation demands conversion of 1.5 M CO_2 into HCO_3^-) for an NH_3 concentration of 3.3 M. Bicarbonate concentration shown for reference as this is important for induction. Error bars indicate standard deviation obtained from sacrificial experiments carried out in triplicate for each ammonia concentration.

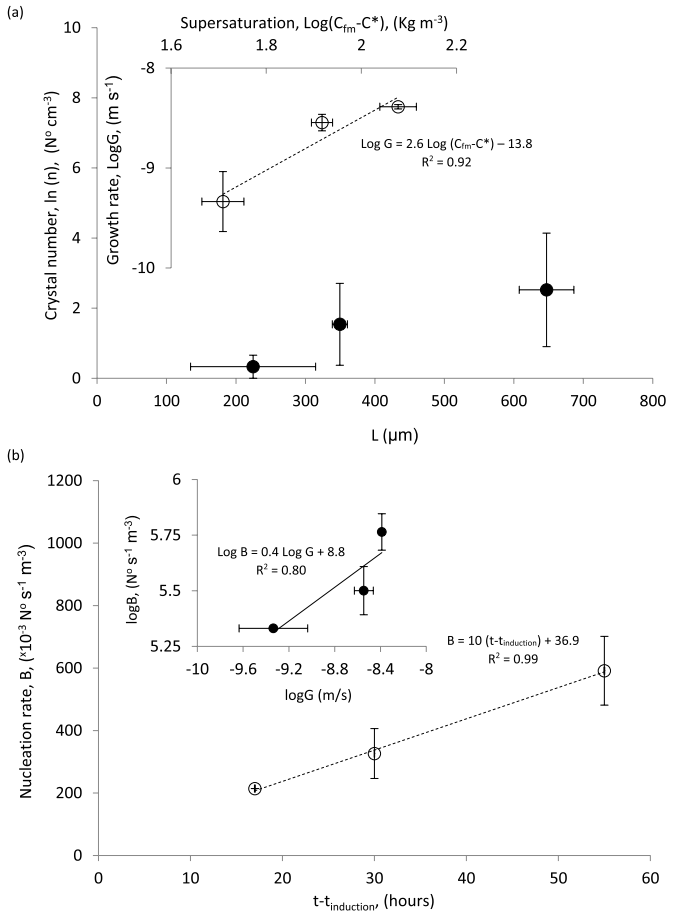

Fig. 8. (a) Crystal population density versus crystal size observed at progressively increasing levels of supersaturation, and inset the determination of crystal growth rate from this data; (b) nucleation rate determined from the onset of induction and inset, the relationship between nucleation rate and growth rate is evaluated.

apparently independent of NH_3 concentration (Fig. 3) which implies the liquid phase imparted negligible resistance to mass transfer, as is commonly reported for chemical absorption where the reactant is in excess [35]. However, a two-stage decline in CO_2 flux was observed following progressive CO_2 absorption. In the initial phase of CO_2 absorption, carbamic acid forms alongside ammonium carbonate [5,28,36]. The carbamic acid deprotonated to form carbamate (Equation (12)), whilst a fraction of the CO_2 reacted with hydroxide to form bicarbonate (HCO_3^-), the cumulative effect being a reduction in solution pH [28] (Fig. 5a). The lower pH shifted the equilibrium toward NH_4^+ (Fig. 2) which is favourable for crystallisation (Equation (1)) but reduced the rate of reaction with CO_2. The onset of the second slower phase of CO_2 flux decline occurred at a pH of between 8.2 and 8.5 for each NH_3 concentration studied (Fig. 5b) which corresponded to a shift in equilibrium from NH_3 to NH_4^+ prior to supersaturation. It is this reduction in reactivity which constrained nucleation rate. The rate of pH decline was dependent upon CO_2 loading (CO_2/NH_3, Fig. 5b) where a relative excess of CO_2 drives a faster decline in pH as was observed in this study with a lower NH_3 absorbent concentration. The subsequent decline in the 'second-stage' of absorption which tended toward a flux of zero for the lower NH_3 concentrations, occurred at a solution pH of less than 7.5, and can be attributed to a complete shift in ammonia-ammonium equilibria to NH_4^+, forcing the reactivity of solution to zero (Fig. 3). The 4.6 M NH_3 solution therefore sustained a higher pH at supersaturation which subsequently favoured HCO_3^- formation at induction (Fig. 6b). We suggest that it is the increased availability of HCO_3^- provided by the buffering capacity of the 4.6 M NH_3 solution which increased nucleation rate and induced surface scaling.

The thermodynamics of the crystalline reaction product were

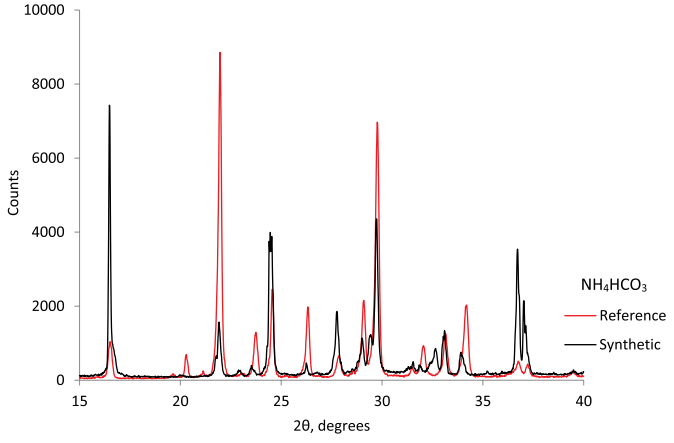

Fig. 9. X-Ray Diffraction (XRD) analysis for comparison of pure ammonium bicarbonate (Reference) with the ammonium bicarbonate produced from chemically reactive membrane crystallisation (Synthetic) using 3.3 M NH_3 solution.

evaluated by Jänecke [37] who identified that the intermediate solid products, ammonium carbonate monohydrate ($[NH_4]_2CO_3H_2O$), sesquicarbonate ($[NH_4]_2CO_3\ 2NH_4HCO_3$) and ammonium carbamate (NH_2COONH_4) could form before the final reaction product (ammonium

bicarbonate) dependent upon solution temperature and CO_2 loading (the molar ratio of CO_2/NH_3). The authors identified that at an absorbent temperature of 5 °C, a CO_2/NH_3 loading exceeding 0.53 was required to induce crystallisation of ammonium bicarbonate (27% NH_3 [37]). In this study, this CO_2 loading was exceeded at each ammonia concentration (Fig. 5b), however, crystallisation did not occur for NH_3 concentrations below 3.3 M. For 1 M absorbent, the solid phase transition is thermodynamically limited since the free ammonia concentration is below the solubility limit for NH_4HCO_3 of 1.5 M (5 °C [38]). At 1.9 M, NH_3 is not thermodynamically limiting. Instead the solid phase transition is kinetically limited by the pH transient which forces the equilibrium toward carbonic acid (H_2CO_3, Fig. 3) such that upon reaching supersaturation (C/C* ~1), there is an insufficiency of bicarbonate to initiate heterogeneous nucleation (Fig. 6). For NH_3 concentrations of 3.3 and 4.6 M, the excess NH_3 reduced the CO_2/NH_3 ratio [28] and sustained pH through to supersaturation such that sufficient HCO_3^- was available to induce crystal growth at CO_2 loadings of 0.77 and 0.44 respectively. Confirmation of crystalline ammonium bicarbonate was provided by XRD analysis. The governance of this kinetic trajectory is in contrast to the thermodynamic description of NH_3–CO_2–H_2O crystallisation where NH_3 concentrations up to 27% wt. have been studied [10, 37]. In such cases, the NH_3 concentration is sufficient to sustain pH, and favour the crystallisation of the more soluble intermediate solid products of ammonium carbonate (320 g l^{-1}) and ammonium carbamate (790 g l^{-1}). Mani et al. [5] identified a similar NH_3 concentration (2.5 M) as the best compromise between CO_2 loading and ammonia slip for packed columns. As demonstrated in this study, a similar ammonia concentration of 3.3 M permits maximum attainable flux to be achieved which will limit membrane area, whilst assuring continuity in the crystallisation of the ammonium bicarbonate product of reaction.

5. Conclusions

In this study, the kinetics and solution chemistry underpinning the chemically reactive membrane crystallisation reactor for gas-liquid absorption of CO_2 into ammonia has been described and the method to recover crystalline ammonium bicarbonate as the reaction product has been demonstrated:

- The two-stage decline in CO_2 flux caused by the reduction in solution pH and the subsequent shift in ammonia-ammonium and carbamate-carbonate-bicarbonate equilibrium demonstrated that a minimum free ammonia concentration is demanded to sustain pH to ensure there is sufficient bicarbonate in the reaction zone at supersaturation to facilitate heterogeneous nucleation.
- Free ammonia concentration greater than 1.9 M did not improve CO_2 flux, which is similar to observations in CO_2–NH_3 packed column investigation. Selection of the upper threshold for ammonia should therefore be based on limiting nucleation rate to avoid crystallisation induced scaling of the membrane.
- Increase in crystal population density and crystal size is indicative of the membrane acting as a physical substrate for heterogeneous nucleation during chemically reactive crystallisation.
- Both nucleation rate and crystal growth rate increased with progressing levels of supersaturation, which can be ascribed to the relatively low chemical reactivity and the unique counter diffusion mechanism fostered by this type of membrane crystallisation technology which provides continued reactant replenishment within the boundary layer where heterogeneous nucleation is promoted by the membrane through reduction in the free energy barrier.
- Provided an appropriate nucleation rate was specified, only limited crystals were observed to form at the membrane and were instead collected downstream of the membrane. Use of sacrificial experiments (i.e. replicates) at each level of supersaturation helped to evidence that consistent and reproducible crystallisation is achievable in this chemically reactive system, indicating limited maintenance intervention should be required.

Integration of the system for simultaneous crystallisation and gas treatment will require progress toward continuous crystallisation through metastable control, or the implementation of multi-stage gas treatment, where the latter option is most likely to achieve the higher crystal product yield.

Declaration of competing interest

The authors declare that they have no known competing financial interests or personal relationships that could have appeared to influence the work reported in this paper.

Acknowledgements

The authors would like to thank our industrial sponsors: Anglian Water, Northumbrian Water and Severn Trent Water for their financial and technical support. We are further grateful for financial support from the Engineering and Physical Sciences Research Council (EPSRC) received through the STREAM Industrial Doctorate Centre and for a Cranfield School of Water, Energy and Environment PhD bursary.

Appendices.

Appendix A. Carbonic acid, bicarbonate and carbonate equilibria

The distributions of carbonic acid, bicarbonate and carbonate vs. pH (Fig. 2a) have been evaluated through the following equations [26,39]:

$$\frac{[H_2CO_3]}{C_T} = \frac{[H^+]^2}{[H^+]^2 + K_{-2}[H^+] + K_{-1}K_{-2}} \quad (A1)$$

$$\frac{[HCO_3^-]}{C_T} = \frac{[H^+]K_{-2}}{[H^+]^2 + K_{-2}[H^+] + K_{-1}K_{-2}} \quad (A2)$$

$$\frac{[CO_3^{2-}]}{C_T} = \frac{K_{-1}K_{-2}}{[H^+]^2 + K_{-2}[H^+] + K_{-1}K_{-2}} \quad (A3)$$

Where C_T is the sum of the carbonic species fractions in solution ($C_T = 1$), while K_{-1} and K_{-2} are the dissociation constants of bicarbonate and carbonic acid, given by (Equations (7) and (8) [26]):

$$K_{-1} = \frac{[CO_3^{2-}][H^+]}{[HCO_3^-]} \quad \text{(A4)}$$

$$K_{-2} = \frac{[HCO_3^{2-}][H^+]}{[H_2CO_3^-]} \quad \text{(A5)}$$

In particular, at temperature T = 5 °C and salinity S = 0%, $K_{-1} = 2.84 \times 10^{-11}$; $K_{-2} = 3.069 \times 10^{-7}$, [39]. Carbonate and ammonia equilibria are used to estimate respective concentrations of dissolved species according to the pH of solution. Due to the relative simplicity of the solution used, this can be regarded as a reasonable estimate of concentration, due to the limited complexity and total dissolved solids concentration, which may otherwise infer some degree of 'salting out' [48]. The use of UV as a surrogate measure of bicarbonate concentration provided confirmatory evidence of the relative accuracy of estimation, having followed comparable trend to those estimated for the dissolved species.

Appendix B. Dissociation of ammonia and ammonium ion

The equilibrium between unprotonated ammonia and protonated ammonium as a function of pH has been evaluated as follows [40]:

$$\alpha_{NH_3} = 1 \Big/ \left(1 + 10^{pK_a^S - pH}\right) \quad \text{(A6)}$$

$$\alpha_{NH_4^+} = 1 - \alpha_{NH_3} \quad \text{(A7)}$$

Where pK_a^S is given by Ref. [41]:

$$pK_a^S = -\log K_a^S = \frac{A}{T} + B \quad \text{(A8)}$$

Specifically, A = 2727.42 and B = 0.0973, respectively, while T is temperature in K [41].

Appendix C. Illustration of crystals recovered downstream from membrane

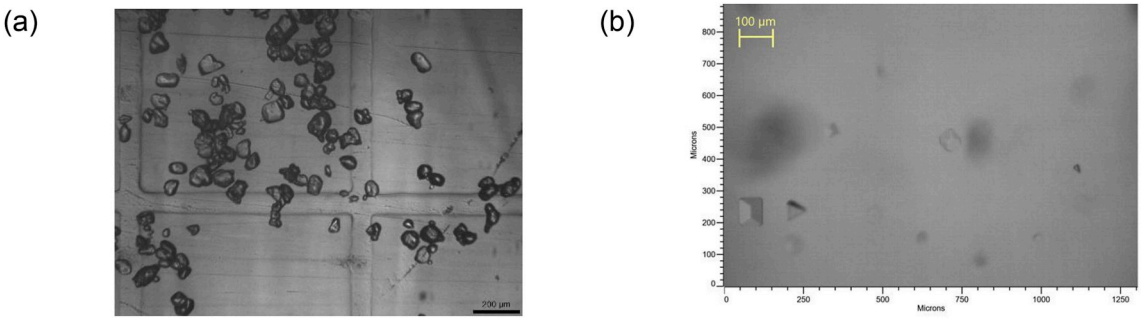

Fig. C1. Example images of crystals downstream of the membrane at early stage of supersaturation: (a) microscope image of crystals, in graded slide; (b) In-situ microscopic determination of crystals during experimentation which illustrate the classical orthorhombic structure of ammonium bicarbonate.

Appendix D. Influence of gas humidity on lumen side crystallisation

The relative humidity in the gas phase exiting the membrane was 38% (Table 1). Gas-phase crystallisation is thought to proceed through one of two mechanisms: direct reaction between CO_2 and NH_3 'slipped' into the gas phase, or wetting and breakthrough of solvent into the gas phase followed by CO_2 dissolution [2,42,43]. Bavarella [44] observed lumen side crystallisation when ammonia absorbent was used in 'single pass' at a concentration of 2.3 M NH_3, which is below the solubility limit (C/C*, 1) required to facilitate crystallisation within the liquid phase. For equivalent absorbent concentration and hydrodynamic conditions (same gas velocity), which established the same relative gas humidity, lumen side crystallisation was prevented through recycling the absorbent.

References

[1] IEA Bioenergy Task 37. http://task37.ieabioenergy.com/plant-list.html, 2016. (Accessed 28 July 2018).
[2] C. Makhloufi, E. Lasseuguette, J.C. Remigy, B. Belaissaoui, D. Roizard, E. Favre, Ammonia based CO_2 capture process using hollow fiber membrane contactors, J. Membr. Sci. 455 (2014) 236–246.
[3] A. McLeod, P. Buzatu, O. Autin, B. Jefferson, E. McAdam, Controlling shell-side crystal nucleation in a gas–liquid membrane contactor for simultaneous ammonium bicarbonate recovery and biogas upgrading, J. Membr. Sci. 473 (2015) 146–156.
[4] A.C. Yeh, H. Bai, Comparison of ammonia and monoethanolamine solvents to reduce CO_2 greenhouse gas emissions, Sci. Total Environ. 228 (1999) 121–133.
[5] F. Mani, M. Peruzzini, P. Stoppioni, CO_2 absorption by aqueous ammonia solutions: speciation of ammonium carbamate, bicarbonate and carbonate by a 13C NMR study, Green Chem. 8 (2006) 995–1000.
[6] A.R. Veiga, C.E. Calmanovici, M. Giulietti, Operational conditions evaluation in ammonium bicarbonate crystallisation, in: Proceedings of the 14th International Symposium on Industrial Crystallization 65, 1999, pp. 1–12.
[7] Kirk-Othmer, Encyclopaedia of chemical technology 2, 1982, pp. 518–519.
[8] M. Gazzani, D. Sutter, M. Mazzotti, Improving the efficiency of a chilled ammonia CO_2 capture plant through solid formation: a thermodynamic analysis, Energy Procedia 63 (2014) 1084–1090.
[9] D. Sutter, M. Gazzani, M. Mazzotti, Formation of solids in ammonia-based CO_2 capture processes — identification of criticalities through thermodynamic analysis of the CO_2–NH_3–H_2O system, Chem. Eng. Sci. 133 (2015) 170–180.
[10] V. Darde, K. Thomsen, W.J.M. van Well, E.H. Stenby, Chilled ammonia process for CO_2 capture, Int. J. Greenh. Gas Control 4 (2010) 131–136.
[11] D. Sutter, M. Mazzotti, Solubility and growth kinetics of ammonium bicarbonate in aqueous solution, J. Crys. Growth Des. 17 (2017) 3048–3054.
[12] H. Yu, G. Qi, S. Wang, S. Morgan, A. Allport, A. Cottrell, T. Do, J. McGregor, L. Wardhaugh, P. Feron, Results from trialling aqueous ammonia-based post-

combustion capture in a pilot plant at Munmorah Power Station: gas purity and solid precipitation in the stripper, Int. J. Greenh. gas Control 10 (2012) 15–25.
[13] Z. Cui, D. deMontigny, Experimental study of carbon dioxide absorption into aqueous ammonia with a hollow fiber membrane contactor, J. Membr. Sci. 540 (2017) 297–306.
[14] K. Villeneuve, D. Roizard, J.-C. Remigy, M. Iacono, S. Rode, CO_2 capture by aqueous ammonia with hollow fiber membrane contactors: gas phase reactions and performance stability, Separ. Purif. Technol. 199 (2018) 189–197.
[15] A. McLeod, B. Jefferson, E.J. McAdam, Biogas upgrading by chemical absorption using ammonia rich absorbents derived from wastewater, Water Res. 67 (2014) 175–186.
[16] S. Zhao, P.H.M. Feron, L. Deng, E. Favre, E. Chabanon, S. Yan, H. Qi, Status and progress of membrane contactors in post-combustion carbon capture: a state-of-the-art review of new developments, J. Membr. Sci. 511 (2016) 180–206.
[17] G. Di Profio, E. Curcio, E. Drioli, Supersaturation control and heterogeneous nucleation in membrane crystallisers: facts and perspectives, Ind. Eng. Chem. Res. 49 (2010) 11878–11889.
[18] E. Curcio, E. Fontananova, G. Di Profio, E. Drioli, Influence of the structural properties of polyvinylideneflouride (PVDF) membranes on the heterogeneous nucleation rate of protein crystals, J. Phys. Chem. 110 (2006) 12438–12445.
[19] R. Kieffer, D. Mangin, F. Puel, C. Charcosset, Precipitation of barium sulphate in a hollow fibre membrane contactor: Part 1, Investigation of particulate fouling, Chem. Eng. Sci. 64 (2009) 1759–1767.
[20] O. Autin, F. Hai, S. Judd, E.J. McAdam, Investigating the significance of coagulation kinetics on maintaining membrane permeability in an MBR following reactive coagulant dosing, J. Membr. Sci. 516 (2016) 64–73.
[21] J.T. Yeh, K.P. Resnik, K. Rygle, H.W. Pennline, Semi-batch absorption and regeneration studies for CO_2 capture by aqueous ammonia, Fuel Process. Technol. 86 (2005) 1533–1546.
[22] S. Atchariyawut, R. Jiraratananon, R. Wang, Separation of CO_2 from CH_4 by using gas–liquid membrane contacting process, J. Membr. Sci. 304 (2007) 163–172.
[23] N.S. Wilson, R. Morrison, J.W. Dolan, Buffers and Baselines, LC-GC Europe, 2001.
[24] X. Ji, E. Curcio, S.A. Obaidani, G. Di Profio, E. Fontananova, E. Drioli, Membrane distillation-crystallization of seawater reverse osmosis brines, Separ. Purif. Technol. 71 (2010) 76–82.
[25] L. Meng, S. Burris, H. Bui, Development of an analytical method for distinguishing ammonium bicarbonate from the products of an aqueous ammonia CO_2 scrubber, Anal. Chem. 77 (2005) 5947–5952.
[26] F. Millero, R.N. Roy, A chemical equilibrium model for the carbonate system in natural waters, Croat. Chem. Acta 70 (1997) 1–38.
[27] R. Sander, Compilation of Henry's law constants (version 4.0) for water as solvent, Atmos. Chem. Phys. 15 (2015) 4399–4981.
[28] X. Wang, W. Conway, D. Fernandes, G. Lawrence, R. Burns, G. Puxty, M. Maeder, Kinetics of the reversible reaction of CO_2(aq) with ammonia in aqueous solution, J. Phys. Chem. 115 (2011) 6405–6412.
[29] G. Chen, Y. Lu, X. Yang, R. Wang, A.G. Fane, Quantitative study on crystallization-induced scaling in high-concentration direct-contact membrane distillation, Ind. Eng. Chem. Res. 53 (2014) 15656–15666.
[30] O. Söhnel, M. Bravi, A. Chianese, B. Mazzarotta, Growth kinetics of sodium perborate from batch crystallization, J. Cryst. Growth 160 (1996) 355–360.
[31] J. Mydlarz, D. Briedis, Modeling of crystal size distribution in a mixed suspension, mixed product removal crystalliser when growth is size dependent, Sep. Technol. 3 (1993) 212–220.
[32] E. Curcio, A. Criscuoli, E. Drioli, Membrane crystallisers, Ind. Eng. Chem. Res. 40 (2001) 2679–2684.
[33] G. Di Profio, E. Curcio, A. Cassetta, D. Lamba, E. Drioli, Membrane crystallisation of lysozyme: kinetic aspects, J. Cryst. Growth 257 (2003) 359–369.
[34] A.C.M. Franken, J.A.M. Nolten, M.H.V. Mulder, D. Bargeman, C.A. Smolders, Wetting criteria for the applicability of membrane distillation, J. Membr. Sci. 33 (1987) 315–328.
[35] A. Esquiroz-Molina, S. Georgaki, R. Stuetz, B. Jefferson, E.J. McAdam, Influence of pH on gas phase controlled mass transfer in a membrane contactor for hydrogen sulphide absorption, J. Membr. Sci. 427 (2013) 276–282.
[36] C.K. Ahn, H.W. Lee, M.W. Lee, Y.S. Chang, K. Han, C.H. Rhee, J.Y. Kim, H.D. Chun, J.M. Park, Determination of ammonium salt/ion speciation in the CO_2 absorption process using ammonia solution: modelling and experimental approaches, Energy Procedia 4 (2011) 541–547.
[37] E. Jänecke, Über die Löslichkeit von Ammonbicarbonat in Wasser bis zum Schmelzpunkt, Zeitschrift für Elektrochemie 35 (1929) 332–334.
[38] R.H. Perry, D.W. Green, Perry's Chemical Engineers' Handbook, eighth ed., 2007.
[39] F. Millero, Thermodynamics of the carbon dioxide system in the oceans, Geochem. Cosmochim. Acta 59 (1995) 661–677.
[40] A.T. Ukwuani, W. Tao, Developing a vacuum thermal stripping-acid absorption process for ammonia recovery from anaerobic digester effluent, Water Res. 106 (2016) 108–115.
[41] R. Bates, G.D. Pinching, Acidic dissociation constant of ammonium ion at 0°C to 50°C, and the base strength of ammonia, J. Res. Natl. Bur. Stand. (U.S.) 42 (1949) 419–430.
[42] X. Li, E. Hagaman, C. Tsouris, J.W. Lee, Removal of carbon dioxide from flue gas by ammonia carbonation in the gas phase, Energy Fuel. 17 (2003) 69–74.
[43] K. Han, C.K. Ahn, M.S. Lee, C.H. Rhee, J.Y. Kim, H.D. Chun, Current status and challenges of the ammonia-based CO_2 capture technologies toward commercialization, Int. J. Greenh. Gas Control 14 (2013) 270–281.
[44] S. Bavarella, Chemically Reactive Membrane Crystallisation Reactor for CO_2 Separation and Ammonia Recovery (PhD Thesis), Cranfield University, UK, 2018.
[45] O. Autin, H. Sakar, E.J. McAdam, Fluorescence enabled direct visual observation for diagnosis of ultrafiltration membrane fouling by bidisperse sub-micron particle suspensions, Water Environ. J. 32 (4) (2018) 519–526.
[46] A. Mookherji, S.P. Tandon, Influence of concentration on the ultraviolet absorption spectrum of bicarbonate ion in state of aqueous solution, J. Phys. Soc. Japan 21 (1966) 1176–1178.
[47] J. Birkmann, C. pasel, M. Luckas, D. Bathen, UV spectroscopic properties of principal inorganic ionic species in natural waters, Water Pract. Technol. 13 (2018) 879–892.
[48] Y. Jiang, E. McAdam, Y. Zhang, S. Heaven, C. Banks, P. Longhurst, Ammonia inhibition and toxicity in Anaerobic Digestion: a critical review, J. Water Process Eng. 32 (2019), 100899.